SIZE EFFECTS FOR REINFORCED CONCRETE BEAMS STRENGTHENED IN SHEAR WITH CFRP STRIPS

A. Godat[1]; Z. Qu[2]; X. Z. Lu[3]; P. Labossière[4]; L. P. Ye[5] and K. W. Neale[*], M.ASCE[6]

1- Postdoctoral Fellow, Department of Civil Engineering, University of Sherbrooke, Sherbrooke, Québec, Canada, J1K 2R1.
E-mail: Ahmed.Godat@USherbrooke.ca

2- Ph.D. Candidate, Key Laboratory of Structural Engineering and Vibration of China Education Ministry, Department of Civil Engineering, Tsinghua University, Beijing, China.
E-mail: qz@mails.tsinghua.edu.cn

3- Associate Professor, Key Laboratory of Structural Engineering and Vibration of China Education Ministry, Department of Civil Engineering, Tsinghua University, Beijing, China.
E-mail: luxinzheng@263.net

4-Professor, Department of Civil Engineering, University of Sherbrooke, Sherbrooke, Québec, Canada, J1K 2R1.
E-mail: Pierre.Labossiere@USherbrooke.ca

5- Professor, Key Laboratory of Structural Engineering and Vibration of China Education Ministry, Department of Civil Engineering, Tsinghua University, Beijing, China.
E-mail: ylp@tsinghua.edu.cn

6- Professor, Canada Research Chair in Advanced Engineered Material Systems, Department of Civil Engineering, University of Sherbrooke, Sherbrooke, Québec, Canada, J1K 2R1.
E-mail: Kenneth.Neale@USherbrooke.ca

* Corresponding author

ABSTRACT: The principal motivation of this study is to obtain a clear understanding of size effects for FRP shear-strengthened beams. The experimental program consists of seven beams of various sizes grouped in three test series. One beam of each series is used as a benchmark and its behavior is compared with a beam strengthened with a U-shaped CFRP jacket. The third test series includes an additional beam strengthened with completely wrapped external CFRP sheets. The experimental results show that the effective axial strains of the CFRP sheets are higher in the smaller specimens. Moreover, with a larger beam size, one can expect less strain in the FRPs. A non-linear finite element numerical analysis is developed to model the behavior of the CFRP shear-strengthened beams. The numerical model is able to simulate the characteristics of the shear-strengthened beams, including the interfacial behavior between the concrete and the CFRP sheets. Three prediction models available in current design guidelines for computing the FRP effective strain and shear contribution to the shear capacity of the FRP shear-strengthened beams are compared with the experimental results.

Keywords: concrete beams; shear strength; fiber reinforced plastics; experimental data; numerical models; axial strain.

INTRODUCTION

Fiber reinforced polymers (FRPs) are currently emerging as a popular option to repair and strengthen reinforced concrete structures. This strengthening technique usually involves the bonding of a thin layer of FRPs to the concrete surface of the structural element in need of repair. In order to fully develop the potential ductility of reinforced concrete flexural members, it is generally desirable that bending rather than shear govern the ultimate strength. However, shear deficiencies do often exist and in such cases there is a need for strengthening and retrofitting for increased shear capacities. In these situations, the external bonding of FRP stirrups is considered a promising method to increase the shear capacity.

The behavior of reinforced concrete members strengthened in shear with external FRP stirrups is influenced by several parameters. The size of the beam is undoubtedly one of the most important parameters affecting the ultimate capacity of a shear-strengthened beam. However, few researchers have investigated this effect, particularly for specimens that have an effective depth greater than 300 mm (Bousselham and Chaallal 2004). In fact, the importance of this parameter has emerged from the relation established between the required effective bond length and the effective FRP strain (Deniaud and Cheng 2001; Khalifa and Nanni 2001). Furthermore, the size of a beam has a strong influence on the shear resistance of the concrete (Kong and Evans 1998; ASCE 1998). On the other hand, from a review of the published experimental and numerical results, it appears that to date there has been no extensive evaluation of the distribution of axial strains in the FRP composites along their depths. The principal motivation of the experimental program of the present study is for a better understanding of the interaction between the beam size and the axial strains in the FRP sheets, and the corresponding shear capacity.

Finite element analysis can be used to investigate the behavior and all the parameters of shear-strengthened beams. However, experimental results are required to validate the numerical predictions. A survey of the literature shows that assuming a perfect bond between the FRP and concrete substrate generally leads to over-predictions of the ultimate load capacities and stress levels in the shear-strengthened beams (Kaliakin et al. 1996; Arduini et al. 1997; Malek and Saadatmanesh 1998a, 1998b; Kachlakev et al. 2001; Al-Mahaidi et al. 2001; Santhakumar et al. 2004; Elyasian et al. 2006). Most of the published studies conclude that the current models for FRP/concrete interfacial behavior are not capable of accurately accounting for debonding (Wong 2001; Lee 2003). Consequently, there is a great need for developing numerical tools that properly simulate the behavior at the FRP/concrete interfaces for cases where failure is governed by FRP debonding (Godat et al. 2007a; 2007b). In this investigation, our objective is to develop a versatile numerical tool able to predict the response of reinforced concrete beams strengthened in shear with externally bonded FRP composites, while paying a special attention to the interfacial behavior and debonding failure criteria.

In this study, various sizes of CFRP shear-strengthened beams are considered. This investigation includes both an experimental program and a corresponding numerical analysis. The experimental program consists of seven beams grouped in three test series. One beam of each series is used as a benchmark and its results are compared with a corresponding FRP U-jacket strengthened beam. The third series includes an additional beam that is strengthened with completely wrapped CFRP sheets. The numerical analyses are carried out in parallel to the experimental tests with the objective of establishing the ability of the numerical model to properly simulate the response of the shear-strengthened beams. The accuracy of the numerical

model is evaluated by comparing the numerical predictions to the experimental results. The significance of the size of the specimens on the overall behavior is discussed.

EXPERIMENTAL PROGRAM

The experimental program was carried out at the Department of Civil Engineering of Tsinghua University, China (Qu et al. 2005). It involved three series of rectangular reinforced concrete beams with the configurations shown in Fig. 1. Each series included a reference beam and a CFRP U-jacket strengthened beam. The third series included an additional beam strengthened with completely enclosed CFRP jackets. The reference beams are labeled as "RC", followed by a number that denotes the series. The notations U4, U5 and U6 refer to the U-jacket strengthened beams for the first, second and third series, respectively, while W7 identifies the completely wrapped specimen of the third series.

In order to examine the size effects for the FRP shear-strengthened beams, the span L and width b were increased proportionally with the height h of the beams. In addition, the plate width w_f, the FRP spacing s_f and thickness t_f were also increased proportionally with the height h_f of the CFRP U-jackets. The dimensions of the specimens along with the amounts of longitudinal steel for each beam are summarized in Table 1. In this table, a and a_0 are the lengths of the outer and inner shear spans, as illustrated in Figure 1. The nominal shear span-to-depth ratio $(\lambda \equiv a/d)$ was 2.0 for all the beams; it is defined as the distance from the loading point to the center of the support. However, due to the relative large stiffness of the loading plates at the loading point and supports, it is believed that the real shear span-to-depth ratio $(\lambda_r \equiv a_0/d)$ is 1.51.

All beams were cast in a plywood mould from a single batch of concrete and were cured under the same conditions for six days before the mould was stripped. The rectangular cross-sections were then smoothed at the bottom edges to avoid any stress concentrations in the FRP wraps at these locations. The maximum aggregate size was 25 mm. The ages at which the beams were tested varied from 40 to 90 days. The concrete compressive strengths f_c' of all the specimens, together with their tensile strengths f_t, and the properties of the CFRP sheets are listed in Table 2. All specimens had the same flexural reinforcement ratio (A_s / bd). Furthermore, all beams were heavily reinforced in bending to ensure that they would fail in shear. The flexural reinforcement bars were cold drawn deformed steel with a yield strength of 400 MPa. No steel stirrups were installed in the shear span of interest (right shear span); however, sufficient amounts of steel stirrups were placed in the other span (left shear span) to ensure that the failure would occur in the shear span of interest.

Before bonding the composite material to the concrete surface, special care was given to the surface preparation. Sandblasting was used to roughen the concrete surface until the aggregates were exposed. This was followed by compressed air cleaning to remove dust and loose particles. Once the surface was prepared to the required standard, the epoxy resin was mixed in accordance with the manufacturer's instructions. The epoxy resin was set to the concrete surface. Then, the FRP strips were placed against the epoxy resin coating and the resin was squeezed through the roving of the strips with a plastic roller. Large entrapped air bubbles at the epoxy/concrete or epoxy/FRP strips was avoided. During hardening of the epoxy, a constant uniform pressure (about 0.22 N/mm^2) was applied on the FRP surface to ensure a good contact. The preparation was carried out at room temperature.

The strengthening material was a unidirectional carbon fiber sheet. It was applied in evenly spaced U-wrap strips. The number of CFRP layers varied from a single ply ($t_f = 0.111$ mm) in the first series, to double plies ($t_f = 0.222$ mm) in the second series, and three plies ($t_f = 0.333$ mm) in the third series. All strengthened beams had the same CFRP reinforcement ratio ($\rho_f = A_f / bd$). The CFRP sheets were applied perpendicular to the beam axis. The geometrical dimensions of the CFRP sheets are summarized in Table 3. For the U-wrap strengthened beams (U4, U5 and U6), two strengthening schemes were used for each beam specimen. The shear span of interest (right shear span) was strengthened with CFRP in the form of U-shaped strips, while completely wrapped CFRP strips were applied on the other span (left shear span). This was done to induce failure in the shear span of interest. For the beam specimen of the third series (W7), it was strengthened with completely wrapped CFRP strips for both shear spans.

All beams were simply supported and subjected to a monotonic static loading applied at the center of the beam. Vertical displacements were measured at the center of the span using linear variable differential transformers (LVDTs). The strains in the CFRP strips were also measured, on the vertical face of the strengthened specimens, in order to estimate the shear strength contribution of each CFRP stirrup. As illustrated in Fig. 2, the CFRP strips were numbered sequentially along the tested shear span beginning from the support.

NUMERICAL ANALYSIS

A three-dimensional finite element program, ADINA (2005a), was used for the numerical analysis of the seven tested beams. In the analysis, appropriate material models were employed to represent the behavior of the concrete, the steel reinforcement and the CFRP sheets. These are described in detail in the ADINA theory and modeling guide (ADINA 2005b). In addition, to

model the bond behavior at the FRP/concrete interfacial behavior, interface elements that properly represent the local bond stress−slip characteristics and failure were used (Fig. 3). The details of the constitutive models and their implementation into the numerical analysis are described in detail in Godat et al. (2007a; 2007b).

The nonlinear load−deformation behavior of the structure was simulated under displacement-controlled loading conditions, as was the case for the laboratory experiments. In view of the geometrical and loading symmetries, only one quarter of the beam was simulated. Additionally, using the dimensions of the actual strengthened beam of the first series (U4), a precision study was performed. The goal of this study was to ensure that the one-quarter model of the beam did not introduce excessive approximation in the simulations. The complete CFRP wrapping scheme installed in the left shear span was simulated by three different approaches. In the first approach, CFRP sheets completely wrapped the section was carried out. U-wrap strengthening scheme was assumed in the second approach, while the side-bonded scheme was used in the third approach. For these three approaches, the CFRP sheets on the left shear span were fully connected to the concrete. However, the U-jacket strengthening scheme and the interface elements lying in the right shear span (shear span of interest) were kept the same for each of these approaches. The significance of the above findings along with their failure modes are discussed in the following section.

EXPERIMENTAL AND NUMERICAL RESULTS

The results presented in the following sections are in terms of ultimate load carrying capacities, load–deflection relationships, and failure modes. Comparisons are also provided in terms of the CFRP axial strain profiles along the sheet depth.

Ultimate load carrying capacities and failure modes

For the beams of the first series, the smallest among the three series with a span of 900 mm and a depth of 200 mm, flexural cracks were observed experimentally in the control specimen near the mid-span at the bottom of the beam, at a load level of 60 kN. The shear crack began to appear at a load of approximately 75 kN. One main shear crack was located close to the mid-depth and extended towards the bottom and the top edge of the beam. As the load increased, the shear crack widened and propagated up to the final failure at a load level of 159 kN. The mode of failure was shear crushing of the concrete under the concentrated load. This agrees with the findings of other researchers, which state that RC beams with transverse steel fail with a diagonal cracked area, whereas those without web reinforcement fail with one principal diagonal crack.

The failure progress of the control beams at different load levels are summarized in Table 4. This table shows the loads, and their values as a percentage to the failure loads, at the stages of flexural cracking, shear cracking, and failure. In terms of these percentages, we observe that the beams RC1 and RC2 had similar values at the stage of flexural cracking. For the control beam of the third series (RC3), the flexural cracks occurred at a lower load percentage than the previous two beams. Similarly, the shear cracks formed at approximately the same load percentage for the specimens RC1 and RC2, but at a significantly lower level for the control beam of the third series. In summary, the general trend is that as the beam size decreases, the ratio of the load at cracking to that at failure increases.

With regard to the ultimate load carrying capacities of the three control specimens, we observe that the failure load of the control beam of the second series (RC2) was 346% higher than that of the first series, while the ultimate capacity of the control beam of the third series occurred at

loads 923% and 129% higher than those of the first and second series, respectively. The failure modes of the three control beams were similar.

The crack patterns at different load levels for the three control beams are reproduced in Fig. 4. For the control beams RC1 and RC2, prior to the failure, one major shear crack formed in the web of the specimens. The shear cracks propagated from the mid-depth of the beam towards the point of the applied load and the support. In the specimen RC1, minor shear cracks formed close to the support. For the specimen RC3, two major shear cracks were observed in the web prior to failure. The locations at which the major shear cracks formed were similar to those reported for the two previous beams. As the load increased, minor shear cracks occurred along the major shear cracks and support. In fact, more distributed shear cracks were seen in the control beam of the third series (RC3) compared to what was observed for the other control specimens. This can be attributed to the depth increase, which results in a relative decrease of aggregate interlock.

For the strengthened specimen of the first series, U4, it was not possible to observe cracks on the sides of the beam because of the presence of the bonded CFRP sheets. However, during loading a clicking sound occasionally emitted from the beam. The sound increased in frequency as the beam was loaded closer to the maximum load bearing capacity. Other than this, no significant warning signals preceded the sudden failure of the specimen. The governing failure mode was delamination of the CFRP sheets from the sides of the specimen. The debonding initiated at the strip closest to the applied load and propagated to the support while peeling off a thin layer of the concrete. Opening of a shear crack along the depth of the beam induces tension in the CFRP strips bridging the crack. The resistance forces in these strips tend to decrease the crack opening,

making it more difficult for the shear crack to grow. The shear capacity of the member is thus improved.

It is mentioned that in some cases the load is not able to increase beyond the first peak, so the ultimate capacity is reached at the failure of the first strip. In other cases, the maximum load may occur after few strips have already failed. Consequently, first strip failure does not necessarily correspond to the ultimate shear capacity. In this study, after the debonding of the first three strips near the loading point, the splitting failure propagated towards the support while the loading values descended progressively until crushing of the concrete.

The maximum recorded load level for the specimen of the first series was 202 kN. This represents an increase of 28% in the ultimate capacity over the control specimen. Table 5 shows the progress of the debonding failure mode in the bonded U-wrap strips with applied load for the first three strips from the point of the applied load. It can be observed from this table that the loading percentages relative to the failure load for specimen U4 (strengthened specimen of the first series) at the various stages of failure are higher than those of the other strengthened specimens. It should be noted that the increase in the loading percentage at which the failure begins to occur is not consistent with the beam size. For the beams of the second (U5) and third (U6) series, there were 14% and 24% increases in shear capacity for the beams of the second and third series, respectively. On the other hand, the specimen strengthened with fully wrapped strips, W7, showed an improvement in the shear capacity up to 37%. The results indicate that beams strengthened with fully wrapped strips do not show any size effect on the shear capacity.

In Table 6 comparisons between the experimental results and numerical predictions are presented. These show that the numerical model is quite capable of predicting the ultimate load

carrying capacities with a high degree of accuracy. Furthermore, the analysis is able to properly simulate the failure modes that were observed experimentally. For the control specimen of the first series (RC1), the predicted ultimate carrying capacity is 4% greater than the test value. The simulated failure mode is identical to the experimental observation. For the strengthened beam of the same series (U4), the numerical prediction of the ultimate load carrying capacity is 105% of the experimental value; in addition, the proposed model successfully simulates the debonding failure of the CFRP U-strips, which was the dominant failure mode. At the stage of significant stress transfer from the concrete to the bonded CFRP sheets, the predicted debonding initiated at the interface elements at the top edge of the strip beside the load. After removing the debonded interface elements, the analyses were continued and the load increased. As the load was further increased, the interface elements of the second strip delaminated at a few centimeters below the top edge of the CFRP sheet. Delamination then continued towards the top edge. The position of the first delamination of the interface elements corresponds to the experimental observations. The delamination progressed until crushing of the concrete. The maximum load occurred after few strips had already failed, which is identical to the experimental observations.

One interesting point concerning the failure process should be highlighted. For beams strengthened with strips in the U-wrap configuration, debonding always occurs first at the strips nearest the applied load, in advance to those mid-way along the shear span. This study revealed that strips intercepting the shear crack close to their ends had small areas of bonding. Those intercepting the shear crack close to their mid-height showed greater areas of bonding. This results in an instantaneous increase in the load carried in the vicinity, which leads to rapid propagation of the debonding of the FRP sheets over the shear cracks, combined with concrete crushing.

Load–deflection relationships

Comparisons between the numerical and experimental results in terms of load–deflection relationships are obviously important to assess the accuracy of the numerical simulations. Figures 5–8 present such comparisons for the tested beams of the first, second and third series, respectively. As displacement-controlled solutions were adopted in the analyses, the numerical models were able to simulate the post-peak behavior.

First series

The experimental and the numerical load–deflection curves of the first series are plotted in Fig. 5. For the control specimen RC1, both curves for the numerical and tested results are essentially similar before cracking occurs. Small discrepancies in the load–deflection curves are observed in the cracking zone. The measured deflection values corresponding to the maximum load carrying capacity are 1.9 mm and 1.7 mm for the experimental and numerical specimens, respectively. It can be seen that the numerical analysis slightly overestimated the stiffness in the cracking region. For the strengthened specimen U4, the numerical results predict load–deflection trends similar to those of the experiments. The numerical predictions underestimate the experimental maximum deflection by 5%.

For the case considering the actual dimensions of the strengthened beam of the first series (U4), the numerical predictions of the load–deflection relationships compared for the three different approaches assumed for the CFRP sheets in the left shear span are shown in Fig. 6. In this figure, the experimental results are plotted for the sake of comparison. Small discrepancies between the load–deflection behaviors of those approaches are observed (Fig. 6). This in particular is attributed to the fact that debonding of the CFRP sheets on the shear span of interest governed

the failure. For the completely wrapped, U-jacket and side–bonded strengthening schemes implemented in the left shear span, the analytical ultimate loads are higher than the experimental values by 6%, 5% and 5% respectively, while the actual deflections are approximately typical.

Second series

Overall, the numerical load–deflection curve of the control specimen is in good agreement with the experimental data. The numerical analysis of the control specimen, depicted in Fig. 7, conservatively overestimates such behavior. The predicted deflection corresponding to the maximum load is lower by 8%. For the strengthened specimen, the predicted load–deflection curve descends abruptly at about 97% of the maximum deflection of the corresponding tested specimen (Fig. 7). The strengthened beam shows a higher load (for the same deflection) than the control beam. This is attributed to the fact that the CFRP strips provide forces to resist the growth of the shear cracks. There is no significant difference in the response between the experimental and numerical load–deflection curves.

Third series

The numerical predictions of the load–deflection curve of the control specimen show similar behavior to the experimental curve prior to the initial cracking phase, as shown in Fig. 8. This is because the CFRP strips carry little stress before the beam starts to crack. At the stage of excessive cracking and excessive stress transfer between the adherent materials, the numerical curve is stiffer than the experimental trends. Consequently, the maximum numerical mid-span deflection is lower than the test value by 7%. For both strengthening schemes, an excellent agreement is obtained in terms of the load–deflection behavior between the numerical predictions and the experimental data, as seen in Fig. 8. Overall, for the beam with a U-jacket

configuration, U6, the numerical analyses underestimate the maximum deflection by 2%. In the case of the beam with completely wrapped scheme, W7, the numerical predictions of the maximum deflection corresponding to the ultimate load carrying capacity is underestimated by 10%.

It appears that applying a complete FRP wrapping for shear strengthening converts the mode of failure from debonding to rupture of the FRPs. This is observed both in the numerical predictions and experimental tests. This particular strengthening approach is effective in enhancing the load carrying capacity. Additionally, the ultimate failure occurred at a large deflection. This explains the absence of a size effect on the shear capacity of beams strengthened with fully wrapped CFRP strips.

Strain distribution along the FRP sheet depth

In order to verify the influence of the size effect on the contribution of the CFRP sheets to ultimate shear capacity, the CFRP axial strains of the strengthened beams were measured. The numerical model is also successful to assess such results through a comparison with the experimental data. The plots of the axial strains in the CFRP strips are presented in Figs. 9–12. In addition, to avoid crowded graphs and to be able to draw suitable conclusions, the CFRP axial strains are plotted at only two load levels; one at a low load value and the other corresponding to the maximum load.

First series

The presented experimental strain profiles shown in Fig. 9(a)–9(c) are for the strips F1, F2 and F3, respectively. For the strip near the support F1 (Fig. 9a), little axial strain in the CFRP strip was observed prior to cracking (not shown). With the load increase, the maximum axial strain is

measured at the bottom edge of the CFRP strip. The profile of the axial strain along the CFRP strip depth is similar to the behavior in a direct shear test. The axial strain descends progressively towards the top end of the CFRP sheet. On the other hand, the axial strain profile along CFRP strip F2 (Fig. 9b) showed the peak strain value beside the bottom end of the CFRP sheet. The numerical and experimental results are similar with approximately zero and a small value at the top edge and bottom edge of the CFRP strip, respectively. The experimental axial strain profiles were not smooth; this is attributed to the crack presence.

The experimental and numerical axial strain profiles along the depth of strip F3 are presented in Fig. 9(c). At a low stress level and a small crack size, we observe a profile similar to the classical strain distribution along the strip depth. As the load is further increased, the ultimate axial strain is found near the mid-depth of the sheet. These results show that the maximum axial strain and the interfacial slip along the sheet depth are observed at the same location. It can be concluded that the maximum axial strain in this CFRP strip at failure is 0.0038, which is 24% of the ultimate strain in the CFRP sheet. Furthermore, the numerical results show that when the debonding occurs, the axial strain degrades to small values in the debonded regions. Based on the results in this study, we can conclude that the maximum axial strain readings are obtained along the shear crack.

Second series

For specimen U5, similar trends as for specimen U4 are observed for strip F1 and F2. Figure 10 shows the axial strain in CFRP strip F3, which is located at midway of the shear span. The experimental axial strain profile along the depth is non-uniform, as was the corresponding strip of specimen U4. This is due to numerous shear cracks. Both the numerical and the experimental

results showed the location of the maximum axial strain to be consistent with the maximum interfacial slip location. This is explained by the fact that the shear crack intercepted the CFRP strip in this region and, consequently, the maximum axial strain was recorded. The maximum experimental axial strain is 0.0036, which is 24% of the ultimate CFRP strain.

Third series

The axial strain profile of strip F3 for specimens U6 and W7 are presented in Figs. 11 and 12, respectively. Similarly, the same behavior as for the aforementioned strengthened specimens, U4 and U5, is observed for specimen U6. The numerical predictions produce similar results as the experimental data. In this case, the evaluated axial strain is 20% of the ultimate axial CFRP strain. As can be seen from Fig. 12, the completely wrapped CFRP sheets showed its superiority over the U-jacket strengthening scheme. The maximum axial strain is 0.012, which is 80% of the ultimate strain. The numerical predictions are in very good agreement with the experimental results.

In summary, as the dimensions of the beams as well as the dimensions of the CFRP strips increased proportionally, the contributions of the CFRP strips is higher in the smaller specimens. Therefore, with a larger beam size, one can expect less improvement of the shear capacity with FRPs. Also, we can conclude that the CFRP strip near the middle of the shear span is intersected by a wide shear crack, and hence more stretched than the other strips. As a result, the maximum axial strain in the FRP occurs at this location.

COMPARISON OF TEST RESULTS WITH DESIGN GUIDELINES

Following the previous discussion on the behavior and failure modes of shear-strengthened beams, it is of interest to see how the measured shear capacity compares with the predictions

from available design guidelines. Three design guidelines are considered in this study; these are ACI (2008), *fib* (2001) and BS (2000). In all these codes of practice, an effective strain (ε_{fe}) is first calculated, then the shear capacity contributed by the FRP (V_f) is obtained. The material safety factors are included in the calculation of such values. The predicted values from each design approach will be compared with the experimental results. The various approaches will first be summarized.

Summary of design equations from various guidelines

ACI design equation

The FRP shear contribution after taking into account a shear crack angle equal to 45° can be written as:

$$V_f = A_f \varepsilon_{fe} E_f (\sin\alpha + \cos\alpha) d_f / s_f \quad (1)$$

where α is the stirrups inclination angle; A_f is the area of the FRP sheets, $A_f = 2nt_f w_f$; n, t_f and w_f are the number of layers, the thickness and width of the FRP sheets, respectively; ε_{fe} is the effective strain in the FRP sheets attained at the section failure; E_f is the tensile modulus of elasticity of the FRP sheets.

ACI adopts an equation based on a bond mechanism to obtain the effective FRP strain (ε_{fe}) when debonding is the governing failure mode. The bond capacity basically depends on the effective bond length (L_e) and the concrete compressive strength (f_c'). The effective bond length is related to the stiffness of the FRP sheet by:

$$L_e = \frac{23300}{(nt_f E_f)^{0.58}} \quad (2)$$

The modification factors, k_1 and k_2, which account for the concrete strength and type of wrapping scheme used are expressed as follows:

$$k_1 = (\frac{f_c'}{27})^{2/3} \tag{3}$$

$$k_2 = \frac{d_f - L_e}{d_f} \quad \text{for U-wraps} \tag{4}$$

$$k_2 = \frac{d_f - 2L_e}{d_f} \quad \text{for side-bonded sheets} \tag{5}$$

where d_f is the depth of FRP sheets measured at the level of longitudinal steel reinforcement. The bond-reduction coefficient (k_v) and the effective FRP strain (ε_{fe}) are computed as:

$$k_v = \frac{k_1 k_2 L_e}{11900\varepsilon_{fu}} \tag{6}$$

$$\varepsilon_{fe} = \min(k_v\varepsilon_{fu}, 0.75\varepsilon_{fu}, 0.004) \tag{7}$$

ε_{fu} is the ultimate tensile strength of FRP. For the fully wrapped configuration, the effective FRP strain is simply limited by the following expression:

$$\varepsilon_{fe} = \min(0.75\varepsilon_{fu}, 0.004) \tag{8}$$

fib design equation

The *fib* design equations use the findings of Triantafillou and Antonopoulis (2000), which express the effective FRP strain in terms of the concrete compressive strength (f_c'), FRP elastic modulus (E_f) and FRP reinforcement ratio (ρ_f). Two best-fit expressions are derived from two separate sets of experimental data for debonding failure and fiber rupture. For the side-bonded

and U-wrap schemes, both debonding failure and fiber rupture are considered as possible failure modes and hence the lower value obtained from the expressions is adopted; it is given by:

$$\varepsilon_{fe} = \min(0.65(\frac{f_c'^{2/3}}{E_f \rho_f})^{0.56} * 10^{-3}, 0.17(\frac{f_c^{2/3}}{E_f \rho_f})^{0.30} \varepsilon_{fu}) \quad (9)$$

For the fully wrapped scheme, fiber rupture is taken to control the final failure and the expression corresponding to this failure mode applies. The effective FRP strain is determined as follows:

$$\varepsilon_{fe} = 0.17(\frac{f_c'^{2/3}}{E_f \rho_f})^{0.30} \varepsilon_{fu} \quad (10)$$

The FRP contribution to the shear capacity is obtained by the following equation after the effective strain is computed:

$$V_f = 0.9 \frac{k\varepsilon_{fe}}{\gamma_f} E_f \rho_f b_w d(\cot\theta + \cot\alpha)\sin\alpha \quad (11)$$

where b_w, d, θ and α are the width of the beam web, effective depth, inclination of the diagonal crack, and principal fiber orientation, respectively; k is the reduction factor to obtain the characteristic FRP strain from the mean value ($k = 0.8$); γ_f is a partial safety factor (γ_f is 1.2 at rupture, and 1.3 at debonding).

The threshold of the effective strain is increased, compared to the other codes, to a maximum value of 0.006.

BS design equation

In this case the ultimate strain in the FRP plies is limited to 0.004. The FRP effective strain (ε_{fe}) is dependent on the failure mode. When the failure mode is rupture of the FRP sheets, the effective strain is:

$$\varepsilon_{fe} = \varepsilon_{fu}(0.5622(E_f\rho_f)^2 - 1.2188(E_f\rho_f) + 0.778) \quad (12)$$

and when the failure mode is debonding of the FRP sheets, the effective strain is computed from:

$$\varepsilon_{fe} = 0.0042((0.835 f_c')^{2/3} w_{fe})/((E_f t_f)^{0.58} d_f) \quad (13)$$

where ε_{fu} is the design ultimate failure strain in the FRP; E_f is the elastic modulus of the FRP sheets in GPa ; ρ_f is the FRP shear reinforcement ratio, given by $(2t_f / b_w)(w_{fe} / s_f)$ for beams strengthened with FRP strips and ($2t_f / b_w$) for beams strengthened with continuous FRP sheets; f_c' is the concrete compressive strength; t_f is the thickness of FRP sheets; w_{fe} is the effective width of the FRP sheets, considered to be related to the strengthening configuration; it is ($d_f - L_e$) for U-wrap schemes and $(d_f - 2L_e)$ for side-bonded schemes; L_e is the effective bond length, given by:

$$L_e = \frac{461.3}{(t_f E_f)^{0.58}} \quad (14)$$

The FRP shear contribution can be calculated by using the same analogy as web steel reinforcement. Shear resistance of the FRP sheets is given by:

$$V_f = \frac{1}{\gamma_{mF}} A_f E_f \varepsilon_{fe} \sin\beta(1 + \cot\alpha)(d_f / s_f) \quad (15)$$

where A_f is the area of the FRP sheets and is equal to $2t_f w_{fe}$; β is the angle of the fiber orientations; d_f is the effective depth of the FRP shear reinforcement, taken as d for rectangular sections, and ($d - slabthickness$) for T-sections; s_f is the spacing between the centers of the FRP strips; in the case of continuous sheets $s_f = w_f$; γ_{mF} is a partial safety factor for the FRP sheets and is equal to 1.4 for CFRP, 1.5 for AFRP and 3.5 for GFRP.

Some comments can be made regarding the guidelines considered. All design codes have provisions to distinguish between FRP debonding and rupture. The ACI method accounts for the difference in strengthening configurations (side-bonded and U-wrap) through the use of different factors. The *fib* and BS codes employ the same equation for these strengthening configurations. In the design of shear-strengthened beams, it is more rational to use different equations for the different repair configurations.

Comparison between test results and predictions from design guidelines

Following the above mentioned design approaches, the FRP effective strain (ε_{fe}) and shear contribution (V_f) for our tested specimens are computed using the various design guidelines and summarized in Table 7 along with the corresponding experimental values. The experimental FRP shear contribution is obtained by subtracting the shear capacity of the control beam (which represents the shear contribution by concrete and steel stirrups) from the capacities of the strengthened beams. It is of interest to mention that when the effective strain calculated by the various design codes increase the threshold of the maximum strain, the limit of the maximum strain is considered.

The ACI design approach overestimates the effective strain for the U-wrap configuration. For the fully wrapped configuration, this design method provides reasonable accuracy compare to the experimental measurements. According to the above findings shown in Table 7, the *fib* guidelines provide identical values of effective strain for all the U-wrapped beams. This may be attributed to the effective strain in this design code, which is based on the FRP reinforcement ratio (this was identical in all the tested specimens). The *fib* method appears to overestimate the effective strain for the U-wrap specimens; however, it underestimates the value for the fully wrapped specimen. Based on the present results, only the BS equation is able to give reasonable predictions for the effective strain of the U-wrapped strengthened specimens; however, this equation tends to underestimate the effective strain for the completely wrapped configuration.

For the smaller specimen (h=200 mm), the three design guidelines (ACI, *fib* and BS) give FRP shear contributions that are very close to the experimental measurements. However, all the design codes overestimate the FRP shear contribution for the midsize specimen (h=400 mm). The ACI design code appears to provide a reasonable value for the large specimen (h=600 mm) with the U-wrap configuration. The other two design codes underestimate the FRP shear contribution with a relatively high discrepancy. For the fully wrapped specimen, all the design expressions show poor agreement with the experimental value; the predicted values are much lower than the test results.

CONCLUSION

The experimental program presented here investigated the shear performance of rectangular reinforced concrete beams strengthened with CFRP U-strips as well as one completely wrapped with FRPs. The size effect was examined for these beams with varying depths. The experimental

program was conducted to obtain a better understanding of the behavior and to improve the database of the influence of the depth size to the ultimate load carrying capacity. Within the indicated scope of this investigation, the particular conclusions emerging from this study are summarized as follows:

- For the control beams, it is observed that for the smaller beam dimensions, a higher loading percentage is attained before the cracking phase.
- The experiment also supplied valuable information on the effect of the depth increase. An increase in depth size is consistent with excessive shear cracks prior to failure.
- The axial strain in the CFRP sheets is not uniformly distributed along their heights. The strip nearest the support showed a response similar to the direct shear test.
- The results confirm that the contributions of the CFRP strips are higher in the smaller specimens. Therefore, with a larger beam size, FRPs provide less improvement in the shear capacity.

Numerical modeling was carried out in parallel to the experimental tests to address the behavior of the beams in more detail. A nonlinear constitutive model was incorporated to represent the interfacial behavior between the concrete and CFRP sheets. The comparison between the numerical predictions and experimental results presents accurate results in terms of the ultimate load carrying capacity, load–deflection relationship and failure modes. Based on the numerical results, the following conclusions are drawn:

- Considering the FRP/concrete interfacial behavior is viable and is necessary to assess the debonding phenomenon.
- The maximum axial strain in the CFRP strips is concentrated along the shear crack. The strip located at the middle of the shear span has the highest axial strain value.

- A consistency is observed between the shear crack locations and the maximum values of the interfacial slips; the delamination occurs over the main diagonal shear crack.

The FRP effective strain measured from the experimental tests, together with the shear contribution are compared to the predictions from the ACI, *fib* and BS design expressions. For the U-wrap specimens, the design equation proposed by the BS estimated the effective strain with good accuracy; however, the ACI method predicted reasonable results for the fully wrapped scheme. For the FRP shear contribution, the ACI equation is believed to be the most appropriate for practical design. However, for the fully wrapped scheme, the ACI method appears to predict the FRP shear contribution with a relatively high discrepancy. It is essential to emphasize that a new design expression should be developed taking various other parameters into consideration such as the steel stirrups, shear span-to-depth ratio, and the width ratio between the FRP and concrete beam.

ACKNOWLEDGEMENTS

This research was funded in part by the Natural Sciences and Engineering Research Council of Canada (NSERC), and the Canadian Network of Centers of Excellence on Intelligent Sensing for Innovative Structures (ISIS Canada). KWN is Canada Research Chair in Advanced Engineered Material Systems, and the support of this program is gratefully acknowledged.

REFERENCES

ACI (2008). *Guide for the Design and Construction of Externally Bonded FRP Systems for Strengthening Concrete Structures,* American Concrete Institute, Michigan, USA.

ADINA (2005a). *Automatic Dynamic Incremental Nonlinear Analysis*, Finite Element Software, Version 8.3. ADINA R&D Inc., Watertown, MA, USA.

ADINA (2005b). *Theory and Modeling guide*, Vol. 1, Chapter 3, Version 8.3. ADINA R&D Inc., Watertown, MA, USA.

Al-Mahaidi, R., Lee, K., and Taplin, G. (2001). ‘‘Behavior and analysis of RC T-beams partially damaged in shear and repaired with CFRP laminates.’’ *Proc., 2001 Structural Congress and Exposition*, ASCE, P.C. Chang, Ed., Washington, DC.

Arduini, M., Nanni, A., Di Tommaso, A., and Focacci, F. (1997). ‘‘Shear response of continuous RC beams strengthened with carbon FRP sheets.’’ *Non-Metallic (FRP) Reinforcement for Concrete Structures, Proc., 3rd Int. Symposium*, Vol. 1, Japan Concrete Institute, Tokyo, Japan, 459-466.

ASCE-ACI Committee 445 (1998). Recent approaches to shear design of structural concrete. *Journal of Structural Engineering, ASCE*, 124(12), 1375-1417.

Bousselham, A. and Chaallal, O. (2004). ‘‘Retrofit of reinforced concrete T-beams in shear with U-shaped CFRP wrap.’’ *Advanced Composite Materials in Bridges and Structures, Proc., 4th International Symposium*, Calgary, Alberta, 8p.

British Concrete Society Technical Report (2000). *Design Guidance for Strengthening Concrete Structures Using Fibre Composite Materials*, The Concrete Society, Berkshire, UK.

Deniaud, C. and Cheng, J. (2001). ‘‘Shear behaviour of reinforced concrete strengthened with FRP sheets.’’ *Canadian Journal of Civil Engineering*, 28(2), 271-281.

Elyasian, I., Abdoli, N. and Ronaph, H. R. (2006). ‘‘Evaluation of parameters effective in FRP shear strengthening of RC beams using FE method.’’ *Asian Journal of Civil Engineering (Building and Housing)*, 7(3), 249-257.

fib (2001). *Externally Bonded FRP Reinforcement for RC Structures*, International Federation for Structural Concrete, Switzerland.

Godat, A., Neale, K.W. and Labossière, P. (2007a). ‘‘Numerical modeling of FRP shear-strengthened reinforced concrete beams.’’ *Journal of Composites for Construction, ASCE,* 11(6), 640-649.

Godat, A., Neale, K.W. and Labossière, P. (2007b). ‘‘Towards modeling FRP shear-strengthened reinforced concrete beams.’’ *Fiber Reinforced Polymer Reinforcement for Concrete Structures, Proc., 8th Int. Symposium*, University of Patras, Patras, Greece.

Kachlakev, D., Miller, T., Yim, S., Chansawat, K. and Postisuk, T. (2001). ‘‘Finite element modeling of reinforced concrete structures strengthened with FRP laminates’’. *Final Report SPR316,* Oregon Department of Transportation Research Group, USA.

Kaliakin, V. N., Chajes, M. J. and Januszka, T. F. (1996). ‘‘Analysis of concrete beams reinforced with externally bonded woven composite fabrics.’’ *Composites Part B:Engineering,* 27(3-4), 235-244.

Khalifa, A. and Nanni, A. (2000). ‘‘Improving shear capacity of existing RC T-section beams using CFRP composites.’’ *Cement and Concrete Composites,* 22 (3), 165-174.

Kong, F and Evans, R. (1987). *Reinforced and Prestressed Concrete*. 3rd Edition, Spon Press, UK, 508p.

Lee, T. K. (2003). ‘‘Shear strengthening of reinforced concrete T-beams strengthened using carbon fibre reinforced polymer (CFRP) laminates.’’ Ph.D. Thesis, Department of Civil Engineering, Monash University, Victoria, Australia.

Malek, A., and Saadatmanesh, H. (1998a). ‘‘Ultimate shear capacity of reinforced concrete beams strengthened with web-bonded fiber-reinforced plastic plates.’’ *ACI Structural Journal,* 95(4), 391-399.

Malek, A., and Saadatmanesh, H. (1998b). ‘‘Analytical study of reinforced concrete beams strengthened with web-bonded fiber reinforced plastic plates or fabrics.’’ *ACI Structural Journal*, 95(3), 343-352.

Qu, Z., Lu, X. Z. and Ye L. P. (2005). ‘‘Size effect of shear contribution of externally bonded FRP U-jackets for RC beams.’’ *Bond Behavior of FRP in Structures (BBFS 2005), Proc., Int. Symposium,* Vol.1, International Institute for FRP in Construction, Hong Kong, China, 363-371.

Santhakumar, R., Chandrasekaran, E. and Dhanarraj, R. (2004). ‘‘Analysis of retrofitted reinforced concrete shear beams using carbon fiber composites.’’ *Electronic Journal of Structural Engineering*, 4, 66-74.

Wong, R. (2001). ‘‘Towards modeling of reinforced concrete members with externally bonded fiber reinforced polymer (FRP) composites.’’ M.Sc. Thesis, Civil Engineering Department, University of Toronto, Toronto, Ontario.

LIST OF TABLES CAPTIONS

Table 1. Geometrical dimensions of tested specimens

Table 2. Material mechanical properties of tested specimens

Table 3. CFRP shear-strengthening dimensions and configurations

Table 4. Failure progress of the control specimens at different load levels

Table 5. Failure progress of the strengthened specimens at different load levels

Table 6. Comparison between experimental and numerical results

Table 7. Comparison of FRP effective strain and shear strength against various design guidelines

Table 1. Geometrical dimensions of tested specimens

No.	Beams sets	Spec.	Beam dimensions (mm) L	b	h	a (mm)	a_0 (mm)	Number of long. steel
1 2	First set	RC1 U4	900	100	200	340	250	$6\phi 12$
3 4	Second set	RC2 U5	1800	200	400	680	500	$6\phi 25$
5 6 7	Third set	RC3 U6 W7	2700	300	600	1020	750	$6\phi 32 + 3\phi 25$

Table 2. Material mechanical properties of tested specimens

No.	Beam set	Specimen	Concrete (MPa) f_c'	f_t	Composites (MPa) Ultimate stress	Ultimate strain
1	First	RC1	51.2	2.55	———	———
2	set	U4	51.2	2.55	3550	0.015
3	Second	RC2	49.7	2.93	———	———
4	set	U5	51.2	2.93	3550	0.015
5	Third	RC3	50.5	3.16	———	———
6	set	U6	51.0	3.16	3550	0.015
7		W7	50.7	3.16		

Table 3. CFRP shear-strengthening dimensions and configurations

No.	Spec.	CFRP dimensions			Strength. type	Strength. details
		t_f (mm)	w_f (mm)	s_f (mm)		
1	U4	0.111	30	20	U-wrap	Vertical strips
2	U5	0.222	60	40	U-wrap	Vertical strips
3	U6	0.333	90	60	U-wrap	Vertical tsrips
4	W7	0.333	90	60	Completely wrapped	Vertical strips

Table 4. Failure progress of the control specimens at different load levels

No.	Spec.	Applied load		Failure
		Flexural cracks	Shear crack	
1	RC1	60 kN (38%)	75 kN (47%)	159 kN
2	RC2	280 kN (40%)	304 kN (43%)	709 kN
3	RC3	433 kN (27%)	516 kN (32%)	1626 kN

Table 5. Failure progress of the strengthened specimens at different load levels

No.	Spec.	Applied load				
		Sound initiation	High sound	Debonding of strip F5	Debonding of strip F4	Debonding of strip F3
1	U4	123 kN (61%)	178 kN (88%)	202 kN (100%)	203 kN (100%)	202 kN (100%)
2	U5	420 kN (52 %)	480 kN (59%)	809 kN (100%)	755 kN (93%)	755 kN (93%)
3	U6	1080 kN (54 %)	1116 kN (55%)	1599 kN (79 %)	1578 kN (78%)	1599 kN (79%)
4	W7	840 kN (38%)	1140 kN (51%)	2048 kN (92%)	2079 kN (94%)	2079 kN (94%)

Table 6. Comparison between experimental and numerical results

No.	Beams sets	Spec.	Experimental results		Numerical results		$P_{num.}$	Failure modes	
			Max. load (kN)	Max. def.[a] (mm)	Max. load (kN)	Max. def. (mm)	$P_{exp.}$	Experimental	Numerical
1	First	RC1	160	1.9	166	1.8	1.04	concrete crushing	concrete crushing
2	set	U4	203	2.2	213	2.1	1.05	deebonding	deebonding
3	Second	RC2	709	3.6	745	3.3	1.05	concrete crushing	concrete crushing
4	set	U5	809	4.2	813	3.9	1.01	debonding	deebonding
5	Third	RC3	1626	6.6	1659	6.1	1.02	concrete crushing	concrete crushing
6	set	U6	2018	6.5	2053	6.4	1.02	debonding	debonding
7		W7	2221	8.4	2203	7.6	0.98	CFRP rupture	CFRP rupture

[a] Deflection measured at maximum load.

Table 7. Comparison of FRP effective strain and shear strength against various design guidelines

	Exp.	ACI	*fib*	BS
Effective strain ε_{fe}				
U4	0.0038	0.0051	0.0054	0.0042
U5	0.0036	0.0048	0.0054	0.0042
U6	0.0032	0.0040	0.0054	0.0036
W7	0.0120	0.0100	0.0080	0.0070
FRP shear strength V_f (kN)				
U4	22	21	16	15
U5	50	82	62	60
U6	196	187	140	127
W7	298	187	168	134

LIST OF FIGURE CAPTIONS

Figure 1. Specimens configurations details

Figure 2. Strip notations along the shear span

Figure 3. Finite element model

Figure 4. Crack patterns of the control specimens at various load levels

Figure 5. Load–deflection relationships for the specimens of the first set

Figure 6. Comparison of load–deflection relationships for specimen U4 with various strengthening configurations

Figure 7. Load–deflection relationships for the specimens of the second set

Figure 8. Load–deflection relationships for the specimens of the third set

Figure 9. Axial strain profiles along the CFRP depth for F1, F2 and F3 bonded strips of specimen U4

Figure 10. Axial strain profiles along the CFRP depth for F3 bonded strip of specimens U5

Figure 11. Axial strain profiles along the CFRP depth for F3 bonded strip of specimen, U6

Figure 12. Axial strain profiles along the CFRP depth for F3 bonded strip of specimen, W7

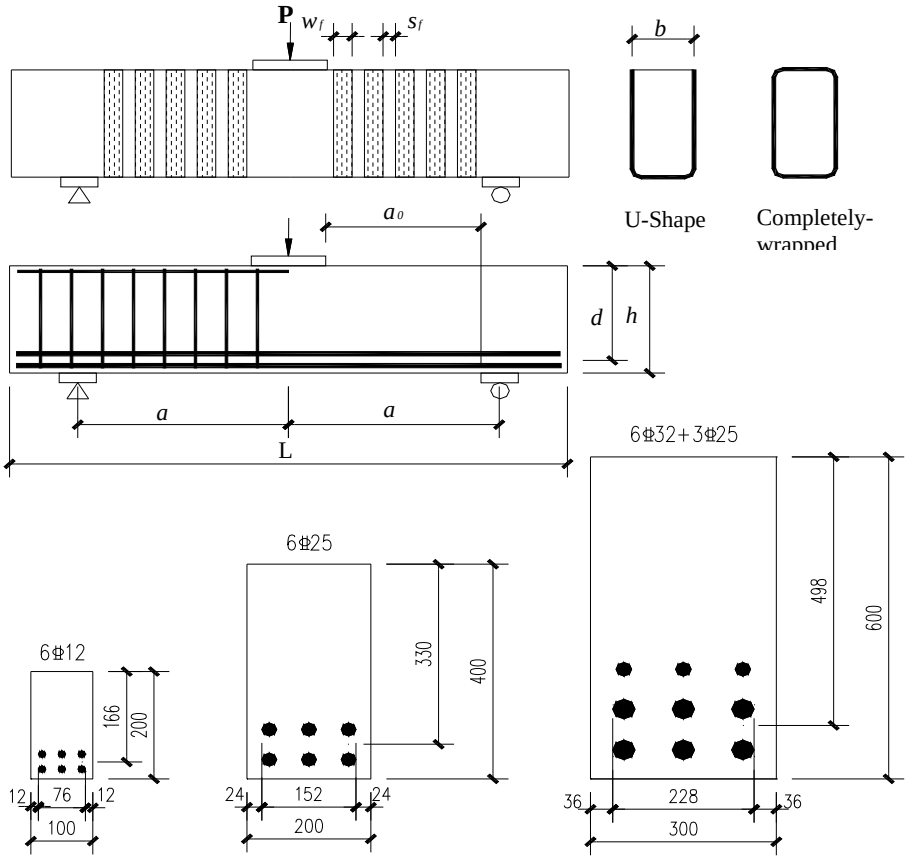

Fig. 1. Specimens configurations details

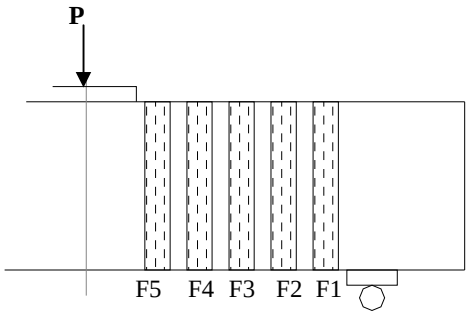

Fig. 2. Strip notations along the shear span

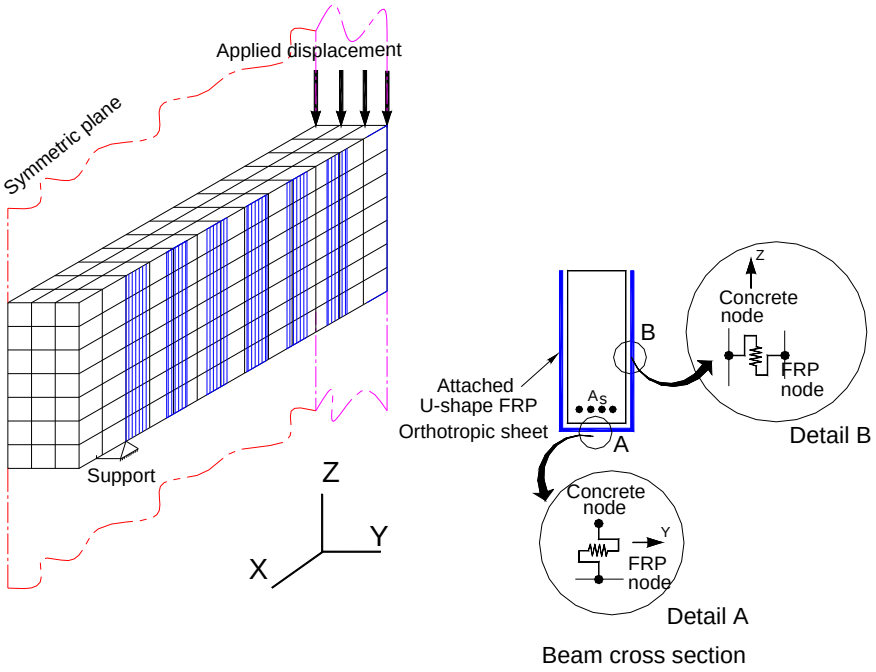

Fig. 3. Finite element model

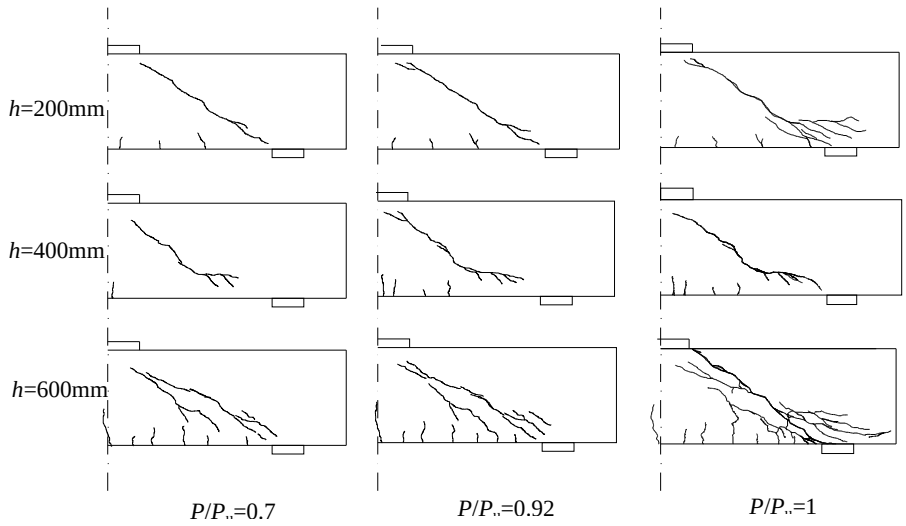

Fig. 4. Crack patterns of the control specimens at various load levels

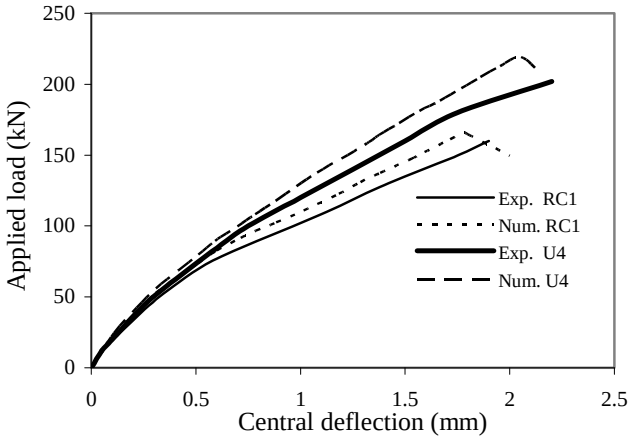

Fig. 5. Load–deflection relationships for the specimens of the first set

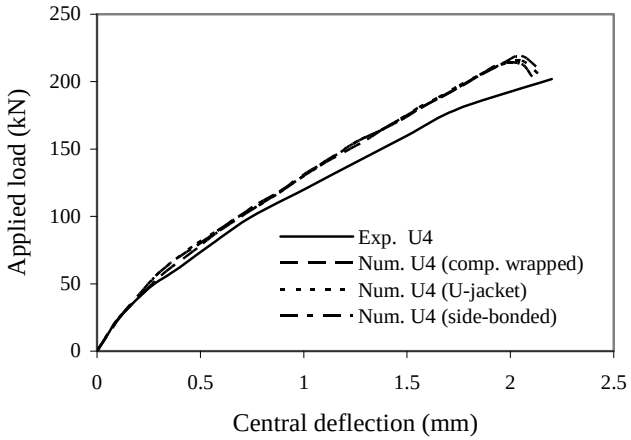

Fig. 6. Comparison of load–deflection relationships for specimen U4 with various strengthening configurations

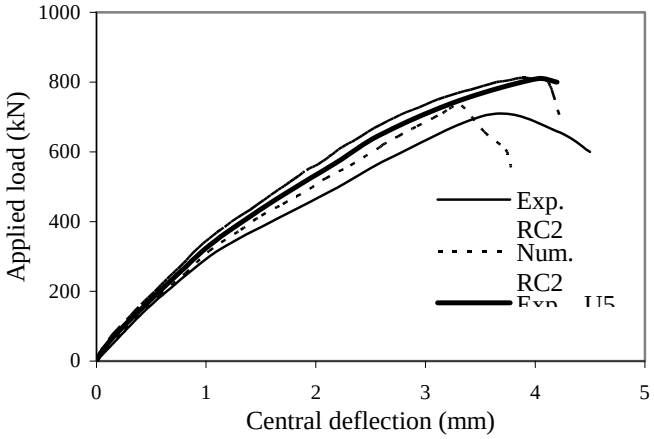

Fig. 7. Load–deflection relationships for the specimens of the second set

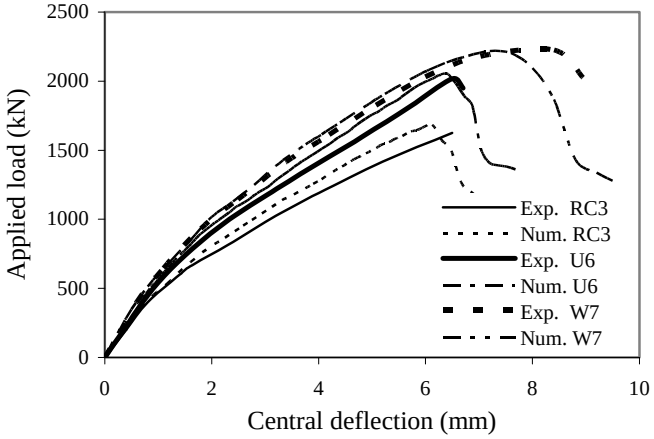

Fig. 8. Load–deflection relationships for the specimens of the third set

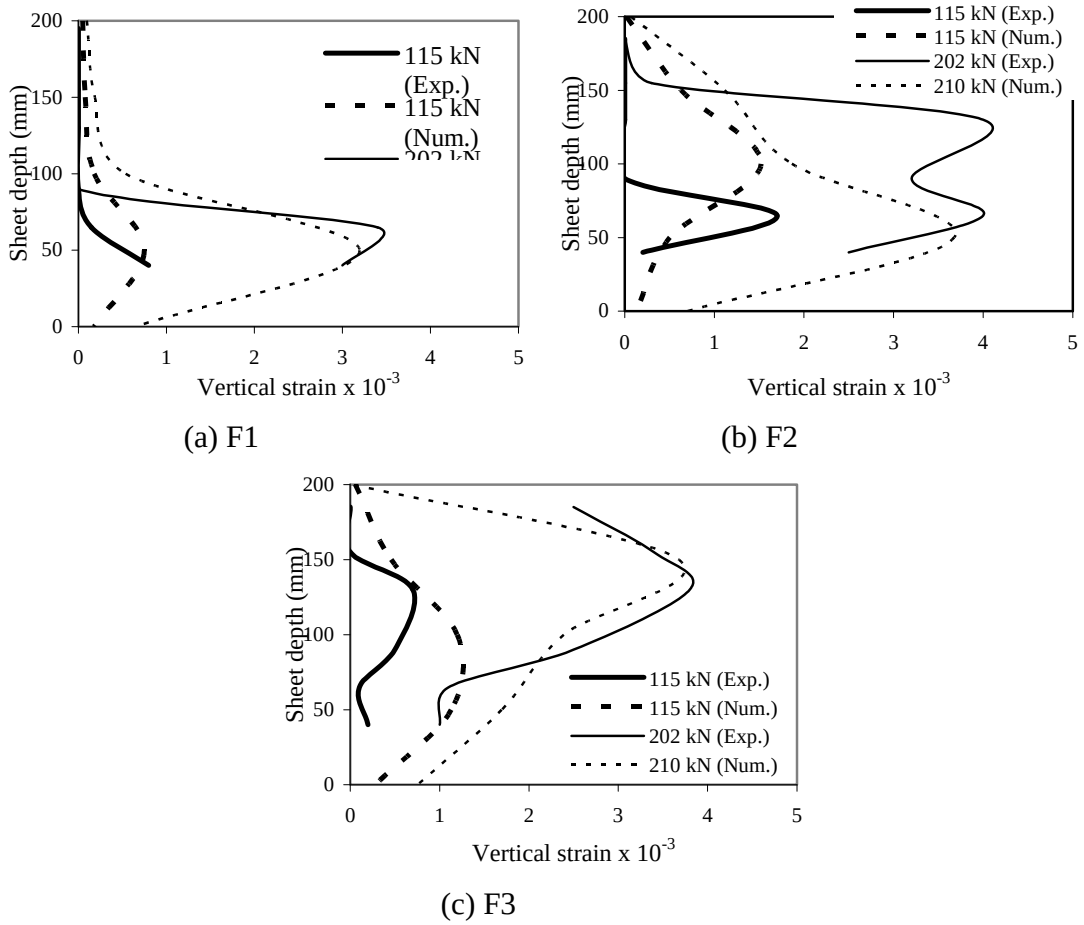

Fig. 9. Axial strain profiles along the CFRP depth for F1, F2 and F3 bonded strips of specimen U4

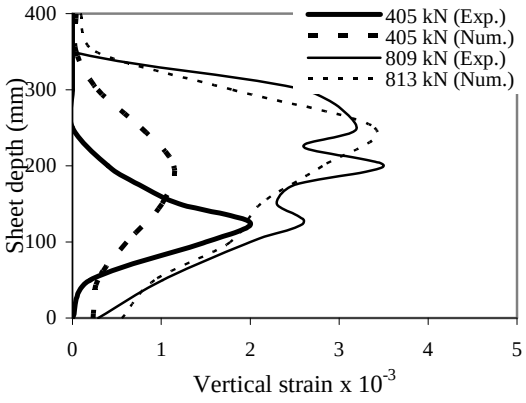

Fig. 10. Axial strain profiles along the CFRP depth for F3 bonded strip of specimens U5

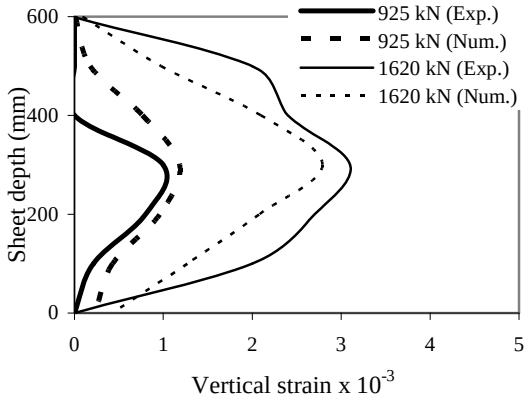

Fig. 11. Axial strain profiles along the CFRP depth for F3 bonded strip of specimen, U6

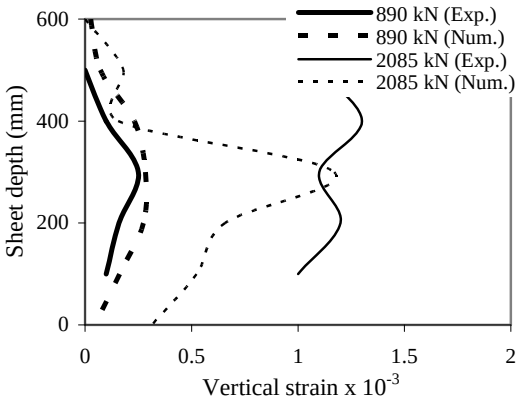

Fig. 12. Axial strain profiles along the CFRP depth for F3 bonded strip of specimen, W7